Clinical & Experimental Immunology
The Journal of Translational Immunology

Clinical and Experimental Immunology ORIGINAL ARTICLE doi:10.1111/cei.13183

Tissue-resident memory T cells are epigenetically cytotoxic with signs of exhaustion in human urinary bladder cancer

C. A. Hartana,* E. Ahlén Bergman,* A. Broomé,* S. Berglund,* M. Johansson,† F. Alamdari,‡ T. Jakubczyk,§ Y. Huge,¶ F. Aljabery,¶ K. Palmqvist,** B. Holmström,†† H. Glise,* K. Riklund,‡‡ A. Sherif§§[1] and O. Winqvist*[1]

*Karolinska Institutet, Department of Medicine Solna, Unit of Immunology and Allergy, Stockholm, †Department of Urology, Sundsvall Hospital, Sundsvall, ‡Department of Urology, Västmanland Hospital, Västerås, §Department of Urology, Länssjukhuset Ryhov, Jönköping, ¶Department of Clinical and Experimental Medicine, Division of Urology, Linköping University, Linköping, **Department of Surgery, Östersund County Hospital, Urology section, Östersund, ††Department of Urology, Akademiska University Hospital, Uppsala, ‡‡Department of Radiation Sciences, Diagnostic Radiology, Umeå University, Umeå, and §§Department of Surgical and Perioperative Sciences, Urology and Andrology, Umeå University, Umeå, Sweden

Accepted for publication 20 May 2018
Correspondence: Ciputra Adijaya Hartana, MD; Department of Medicine Solna, Unit of Immunology and Allergy, Karolinska University Hospital L2:04, 17176 Stockholm, Sweden.
E-mail: ciputra.adijaya.hartana@ki.se

[1]Both senior authors contributed equally to this work

Summary

Tissue-resident memory T (T_{RM}) cells are CD8$^+$ T lymphocytes that reside in the tissues, including tumours. This T cell subset possesses a magnitude of cytotoxicity, but its epigenetic regulation has not been studied. Here, we investigate the impact of perforin DNA methylation in T_{RM} cells and correlate it with their functional potential. Fifty-three urothelial urinary bladder cancer (UBC) patients were recruited prospectively. The DNA methylation status of the perforin gene (*PRF1*) locus in T_{RM} cells was investigated by pyrosequencing. Flow cytometry with ViSNE analysis and *in-vitro* stimulation were used to evaluate T_{RM} cell phenotypes. We discovered that tumour T_{RM} cells have low DNA methylation in the *PRF1* locus (32·9% methylation), which corresponds to increased numbers of perforin-expressing T_{RM} cells. Surprisingly, programmed cell death 1 (PD-1) expression is high in tumour T_{RM} cells, suggesting exhaustion. Following interleukin-15 and T cell receptor stimulation, perforin and T-bet expressions are enhanced, indicating that T_{RM} cells from tumours are not terminally exhausted. Moreover, a high number of T_{RM} cells infiltrating the tumours corresponds to lower tumour stage in patients. In conclusion, T_{RM} cells from UBC tumours are epigenetically cytotoxic with signs of exhaustion. This finding identifies T_{RM} cells as potential new targets for cancer immunotherapy.

Keywords: CD8-positive T lymphocytes, cell exhaustion, DNA methylation, perforin, tissue-resident memory T cells, urinary bladder neoplasms

Introduction

Tissue-resident memory T (T_{RM}) cells are defined as a memory CD8$^+$ T cell subset that does not recirculate. Consequently, T_{RM} cells have a preferential localization in tissues, which has been demonstrated in cancer, infection, allergy and autoimmunity [1]. T_{RM} cells are identified by their surface expression of CD103 (αEβ7 integrin), that binds to E-cadherin expressed on epithelia, and CD69, which antagonizes sphingosine 1-phosphate receptor 1 (S1PR1)-mediated egress from tissues [2]. Both CD103 and CD69 contribute to anchoring of T_{RM} cells in non-lymphoid peripheral tissues [3]. Additionally, CD49a expression has been demonstrated to characterize T_{RM} cells in the human epidermis [4].

The microenvironment in the tissues has been reported to induce the development of T_{RM} cells. One signal reported to play a role is transforming growth factor (TGF)-β1.

TGF-β1 induces CD103 expression through nuclear factor of activated T cells (NFAT)-1 and suppressor of mothers against decapentaplegic (Smad)2/3 transcription factors binding to the promoter region of the *ITGAE* gene, encoding for CD103 [5]. Correspondingly, a similar effect has been demonstrated in TGF-β-rich tumours, in which T_{RM} cells are consequently generated [6].

Reports have demonstrated that a high number of tumour-infiltrating T_{RM} cells is linked to improved prognosis in patients with urinary bladder, lung, cervical and ovarian cancers [7–10]. The improved prognosis is due to the capacity of T_{RM} cells to produce IFN-γ upon *in-situ* antigen recognition [11], resulting in the recruitment of circulating T cells from the blood [12]. Furthermore, the cytotoxic capacity of T_{RM} cells against tumour cells is demonstrated by their production of the cytotoxic mediators, perforin, granzyme A, and granzyme B upon CD103/E-cadherin ligation and T cell receptor (TCR) activation [8]. Notably, the cytotoxic activity of $CD8^+$ T cells is initiated by perforin forming the pore that allows granzymes to enter and induce apoptosis of the tumour cells [13]. In contrast, T_{RM} cells residing in the tumour tissue have been demonstrated to express programmed cell death 1 (PD-1), suggesting exhaustion [14]. In this context, the phenotype of T_{RM} cells displaying simultaneous cytotoxicity and exhaustion markers needs further study.

Here, we investigate the properties of perforin expression in T_{RM} cells, starting at the epigenetic level by means of DNA methylation. DNA methylation is defined as methylation of the cytosine residue in a cytosine–phosphate–guanine (CpG) site [15]. It has been linked to gene silencing due to the inability of transcription factors to bind to the promoter of a particular gene [16]. Moreover, study of the DNA methylation profile from the enhancer region of a gene is more critical. This region contains abundant binding sites for key lineage transcription factors, and enhancer-initiated transcription occurs as the most rapid transcriptional change when cells commence state differentiation [17]. Additionally, epigenetic modification of the lineage-specific enhancer corresponds to lineage-specific cell transcription [18].

In this study we focus upon urothelial urinary bladder cancer (UBC), which in the western world is the fourth most common cancer in men and ninth in women [19]. The non-muscle-invasive UBC is treated routinely using Bacillus Calmette–Guerin (BCG) instillation in the bladder, indicating a substantial level of immunogenicity in this cancer [20]. In this study we investigated the DNA methylation profile of the perforin gene enhancer on T_{RM} cells lodged in the tumour from UBC patients. The study of the DNA methylation profile of this cell subset was accompanied by analysis of the phenotypical properties *ex vivo* and after *in-vitro* stimulation.

Materials and methods

Patient characteristics and tissue collection

Fifty-three patients diagnosed with UBC were recruited prospectively from nine hospitals in Sweden (Umeå University Hospital, Sundsvall-Härnösand County Hospital, Västerås County Hospital, Jönköping/Ryhov County Hospital, Vrinnevi County Hospital in Norrköping, Linköping University Hospital, Östersund County Hospital, Uppsala University Hospital and Skellefteå County Hospital) between 2016 and 2018 (Supporting information, Table S1). All patients underwent diagnostic trans-urethral resection of the bladder (TUR-B) and patients with muscle invasive tumours proceeded to radical cystectomy, with or without preceding neoadjuvant chemotherapy. Peripheral blood (PB) and tumour tissues were acquired at the time of TUR-B, whereas sentinel nodes (SN) and PB were obtained at radical cystectomy. PB was collected in sodium heparin tubes (Greiner Bio-One, Kremsmünster, Austria). SNs were identified perioperatively with detailed mapping, as described previously [21]. Briefly, radioactive tracer ^{99m}Technetium was injected into the area surrounding the tumour or tumour scar during the cystectomy operation. Lymphadenectomies were then carried out and the nodes radioactivity was measured by handheld Geiger counter. Tumour tissue and SN were divided into two parts: one part for routine pathological examination and one part for immunological analysis in this study. The tumour and SN for this study were immersed immediately in RPMI-1640 medium (Sigma Aldrich, St Louis, MO, USA) in 4–8°C and all the samples were processed within 24 h. Buffy coat samples from healthy donors were acquired from Karolinska University Hospital blood bank, Sweden. Informed consent from all patients recruited in this study was obtained in accordance with the Declaration of Helsinki. The study was approved by the regional ethical board (EPN-Stockholm, registration number: 2007/71-31 with amendment 2017/190-32).

Processing of samples

Peripheral blood mononuclear cells (PBMC) were obtained from whole blood samples of patients and healthy donors by density gradient separation using Ficoll-Paque Plus (GE Healthcare, Chicago, IL, USA). Isolated PBMC were suspended in AIM-V medium (Life Technologies, Paisley, UK).

Tumour-infiltrating lymphocytes (TIL) were isolated from the tumour by slicing the collected tissue into small pieces. The small tissues were then transferred into the C-tubes (Miltenyi Biotech, Bergisch Gladbach, Germany) containing 10 ml of AIM-V medium with 1% DNAse I

(Sigma Aldrich) and 1% collagenase/hyaluronidase (StemCell Technologies, Cambridge, UK). Tissues inside the C-tubes were processed in GentleMACS (Miltenyi), according to the manufacturer's protocol. The processed tissue was filtered through a 40-μm cell strainer, washed and suspended in AIM-V medium.

Lymphocytes from SN were isolated by gentle pressure homogenization through a 40-μm cell strainer in AIM-V medium. The cell suspension was washed and suspended in AIM-V medium.

Cell sorting

For the initial DNA methylation site screening, perforin$^+$ and perforin$^-$ CD8$^+$ T cells were isolated from PBMC of healthy donors. First, bulk CD8$^+$ T cells were sorted using EasySep Human CD8 Positive Selection Kit (StemCell Technologies). The selected CD8$^+$ T cells were labelled with anti-CD8 (clone RPA-T8; BD Biosciences, San Jose, CA, USA) and anti-CD56 (clone B159; BD Biosciences) antibodies, followed by fixation in HOPE I Fixation solution (DCS Innovative Diagnostik-Systeme, Hamburg, Germany) overnight in 0–4ºC. The next day, the cells were permeabilized with 0·1% saponin [w/v in phosphate-buffered saline (PBS)] (Sigma Aldrich) and stained intracellularly with anti-perforin antibody (clone δG9; BD Biosciences) for sorting by flow cytometry.

Bulk CD8$^+$ T cells were presorted from patients' PBMC, SN and tumour using the EasySep Human CD3 Positive Selection Kit (StemCell Technologies). The selected cells were subsequently sorted by flow cytometry after cell labelling with anti-CD8 (clone RPA-T8; BD Biosciences) and anti-CD56 (clone B159; BD Biosciences) antibodies. Cells to be sorted were defined as CD8$^+$CD56$^-$.

For sorting of different memory CD8$^+$ T cell subsets, CD8$^+$ T cells were isolated initially from PBMC and tumour of UBC patients using the EasySep Human CD8 Positive Selection Kit. The cells were then labelled with anti-CD8 (clone RPA-T8; BD Biosciences), anti-CD56 (clone B159; BD Biosciences), anti-CD103 (clone Ber-ACT8; BioLegend, San Diego, CA, USA), anti-CCR7 (clone 150503; BD Biosciences) and anti-CD45RA (clone HI100; BD Biosciences) antibodies and sorted by flow cytometry.

Cell sorting by flow cytometry was performed using the fluorescence-activated cell sorter (FACS) Aria I instrument (BD Biosciences) and FACS Diva software (BD Biosciences).

DNA extraction and bisulfite conversion

DNA was extracted and bisulfite converted from frozen pellets of sorted cells using the EZ DNA Methylation Direct Kit (Zymo Research, Irvine, CA, USA), according to the manufacturer's protocol.

TA cloning and bisulfite sequencing

Bisulfite-converted DNA was amplified by polymerase chain reaction (PCR) using Platinum Taq DNA Polymerase High Fidelity (ThermoFisher, Fremont, CA, USA) in a T100 Thermal Cycler (Bio-Rad). The primers used (Eurofins Genomics, Ebersberg, Germany) are listed in Supporting information, Table S2. PCR amplicons were gel-purified using the QIAquick Gel Extraction Kit (Qiagen, Valencia, CA, USA). Next, the PCR amplicons were TA-cloned into pCR4-TOPO vector (ThermoFisher) and transformed into TOP10 *Escherichia coli* (ThermoFisher) by heat shock, according to the manufacturer's protocol. Transformed cells were cultured on lysogeny broth (LB) plates with 50 μg/ml Kanamycin (Substrate Unit, Karolinska University Hospital) and incubated overnight at 37ºC. The following day, 20 colonies were picked from each plate and cultured overnight in LB medium containing 50 μg/ml Kanamycin (Substrate Unit, Karolinska University Hospital) at 37ºC at 210 rpm. Plasmid DNA was extracted using PureLink Quick Plasmid Miniprep Kit (ThermoFisher) and Sanger sequenced using T3 sequencing primer (Supporting information, Table S2) to establish CpG methylation profile on a single cell level.

Pyrosequencing

DNA amplification of the region containing *PRF1* reporter CpG site [–1053 base pairs (bp) upstream of the transcription start site (TSS)] in the enhancer was performed with PCR using Jumpstart REDTaq DNA polymerase (Sigma Aldrich) in T100 Thermal Cycler (Bio-Rad). One of the primers used for amplification was biotinylated (Biomers) (Supporting information, Table S2). Biotinylated PCR amplicons were purified using the Pyromark Q96 Vacuum workstation (Qiagen), followed by pyrosequencing using the Pyromark Q96 ID instrument (Qiagen) with Pyromark Gold Q96 reagent (Qiagen), according to the manufacturer's protocol. Analysis of the data was performed using Pyromark Q96 software (Qiagen) to determine the CpG methylation profile.

Cell culture

For the 5-azacytidine (5-aza) experiment, CD8$^+$ T cells from PB of healthy donors were cultured initially *in vitro* in AIM-V medium supplemented with 200 IU/ml recombinant human interleukin (IL)-2, 5 μg/ml plate-coated anti-CD3 and 1 μg/ml anti-CD28 stimulating antibodies. After 48 h, 5-aza was added to the culture at a final concentration of 2·5 μM/ml for 48 h. The cells were washed and fresh AIM-V medium was added for another

48 h. The cells were kept at 37°C in 5% CO_2 during the culture. At the end of culture, the cells were analysed by flow cytometry.

For the T_{RM} cells activation assay, T_{RM} cells were isolated from PB and tumour of patients. The cells were stimulated *in vitro* in AIM-V medium supplemented with 20 ng/ml

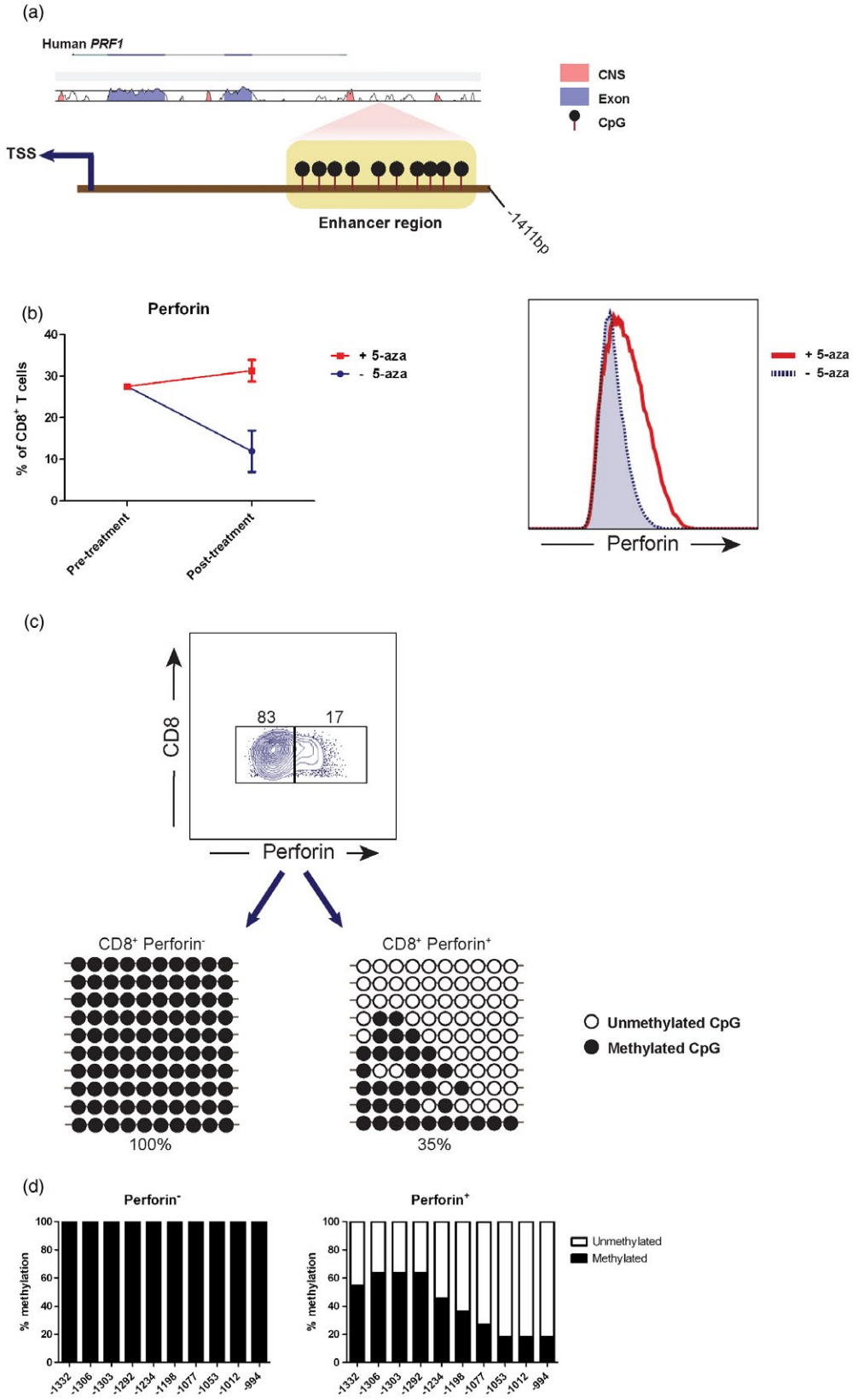

Fig. 1. DNA methylation in the enhancer region regulates perforin transcription. (a) Promoter region sequence containing enhancer in the *PRF1* gene was aligned between human and mouse using the VISTA tool. The conservation degree is indicated by the peaks, with coloured peaks (blue for exon and light red for the non-coding sequence) indicating > 70% conservation. Ten cytosine–phosphate–guanine sites (CpGs) in the enhancer are displayed upstream from the transcription start site (TSS). (b) Sorted $CD8^+$ T cells from healthy donors were cultured initially in the presence of 200 IU/ml recombinant human interleukin (IL)-2, 5 μg/ml plate-coated anti-CD3 and 1 μg/ml anti-CD28 stimulating antibodies *in vitro*. 5-Azacytidine (5-aza) was added to the culture at a final concentration of 2·5 μM/ml for 48 h, followed by culture medium replacement and incubation for another 48 h. Flow cytometry data demonstrating perforin expression pre- and post-treatment are shown. (c) $Perforin^-$ and $perforin^+$ $CD8^+$ T cells were sorted. DNA was extracted and bisulfite-converted from each cell subset, TA-cloned to pCR4-TOPO vector and transformed into TOP10 *Escherichia coli*. Colonies were picked from each cell subset and their DNA was sequenced to measure DNA methylation status of the 10 CpGs in the enhancer. The data display rows represent individually sequenced clone. (d) The bar graphs display total DNA methylation percentage in each CpG from clones in (c).

recombinant human IL-15, 5 μg/ml plate-coated anti-CD3 and 1 μg/ml anti-CD28 stimulating antibodies. The cells were incubated for 48 h at 37°C in 5% CO_2, after which the cells were harvested and analysed by flow cytometry and pyrosequencing.

Flow cytometry

Single cell suspensions isolated from PB, SN and tumour were stained for surface and intracellular markers for flow cytometry analysis. Briefly, cells were stained with fixable live/dead dye (Life Technologies), followed by surface marker staining using anti-CD8 (clone RPA-T8; BD Biosciences), anti-CD56 (clone B159; BD Biosciences), anti-CD103 (clone Ber-ACT8; BioLegend), anti-CCR7 (clone 150503; BD Biosciences), anti-CD45RA (clone HI100; BD Biosciences) and anti-PD-1 (clone EH12.2H7; BioLegend) antibodies. The cells were then fixated and permeabilized using the forkhead box P3 (FOXP3) transcription factor kit (eBioscience, San Diego, CA, USA). Next, the cells were stained for intracellular marker using: anti-perforin (clone δG9; BD Biosciences), anti-granzyme B (clone GB11; BD Biosciences), anti-T-bet (clone 4B10; BioLegend) and anti-Ki-67 (clone 20Raj1; eBioscience) antibodies. Isotype control was used to ascertain the correct gating for the following markers: perforin, granzyme B, T-bet, Ki-67 and PD-1. Flow cytometry data were acquired using an LSR Fortessa instrument (BD Biosciences) and analysed with FlowJo version 10 (TreeStar, Inc., Ashland, OR, USA).

ViSNE

ViSNE was used as a bioinformatic tool to analyse high-dimensional single cell data from flow cytometry. The Barnes–Hut Stochastic Neighbor Embedding (bh-SNE) algorithm was used by the ViSNE tool to map the events. Samples utilized in the analysis were first gated manually using FlowJo version 10 for $CD8^+$ T cells and the data were exported as flow cytometry standard (FCS) files with compensated parameters. The measured fluorescence intensity of the parameters included in the analysis was transformed using the arcsin function with a co-factor of 150. Subsampling was generated randomly from each sample with a total number of cells varying between 2000 and 3000 cells/sample in order to adjust all groups of samples with the same comparable number of events. ViSNE analysis was performed using all parameters that were not subjected to manual gating of $CD8^+$ T cell population. Analysis was perfomed using the tool CYT on the MATLAB (Mathworks) platform [22].

Statistical analysis

For comparison of the two independent groups, a two-tailed independent *t*-test was used for parametric data and the Mann–Whitney *U*-test was used for non-parametric data. One-way analysis of variance (ANOVA) was used to compare the means among three groups or more with parametric data, meanwhile the Kruskal–Wallis test was used when comparing non-parametric data. Normality test was performed using the Kolmogorov–Smirnov test on all the data in this study; SPSS version 23 software (IBM, Armonk, NY, USA) was used for all the statistical analyses.

Results

Perforin expression is regulated by DNA methylation in the enhancer region

The enhancer region of the perforin coding gene, *PRF1*, was identified previously to be located upstream of the TSS (Fig. 1a), and regulates the expression of perforin [23]. This enhancer region is CpG-rich, with 10 identified CpG sites (chr10: 72, 363, 525–72, 363, 863) (Fig. 1a). In order to investigate the evolutionary conservation of the regulatory element in this locus, we aligned human and mouse DNA sequences using the VISTA tool. We found that the enhancer region of the *PRF1* was not conserved evolutionarily between the two species (< 70% conservation) (Fig. 1a). This indicated the greater importance of using a human model to explore DNA methylation of the *PRF1* enhancer. Moreover, instead of using gene silencing analysis, we validated that DNA methylation regulated perforin expression, as displayed when treating $CD8^+$ T

cells with the demethylating agent, 5-aza, which resulted in elevated perforin expression (Fig. 1b).

In order to identify CpGs responsible for regulating perforin transcription, we examined the methylation profile of the 10 CpGs identified in the enhancer region. Bisulfite-converted DNA from perforin$^-$ and perforin$^+$ CD8$^+$ T cells obtained from healthy donors was TA-cloned and sequenced in order to acquire the methylation status from a single cell level. We discovered that in the perforin$^-$ CD8$^+$ T cells, all the CpGs were methylated completely, in contrast to perforin$^+$ cells (35% total methylation) (Fig. 1c), indicating that CpG demethylation in this enhancer is crucial for perforin transcription. The three CpGs closest to the TSS (position –1053, –1012 and –994) were the least methylated in perforin$^+$ CD8$^+$ T cells (Fig. 1d). Correspondingly, CpG in position –1053 was chosen as the reporter for perforin expression.

CD8$^+$ T cells possess distinct cytotoxicity in different tissues by epigenetic regulation

Next, we investigated the methylation profile of the *PRF1* reporter CpG site (–1053) in CD8$^+$ T cells isolated from UBC patients by pyrosequencing of the PCR-amplified bisulfite-converted target locus. We discovered no significant difference between CD8$^+$ T cells from tumour (mean = 44·1%) and PBMC (mean = 46·6%) (P = 0·95) (Fig. 2a). In contrast, CD8$^+$ T cells from SN had higher methylation in the *PRF1* reporter CpG site (mean = 66·8%)

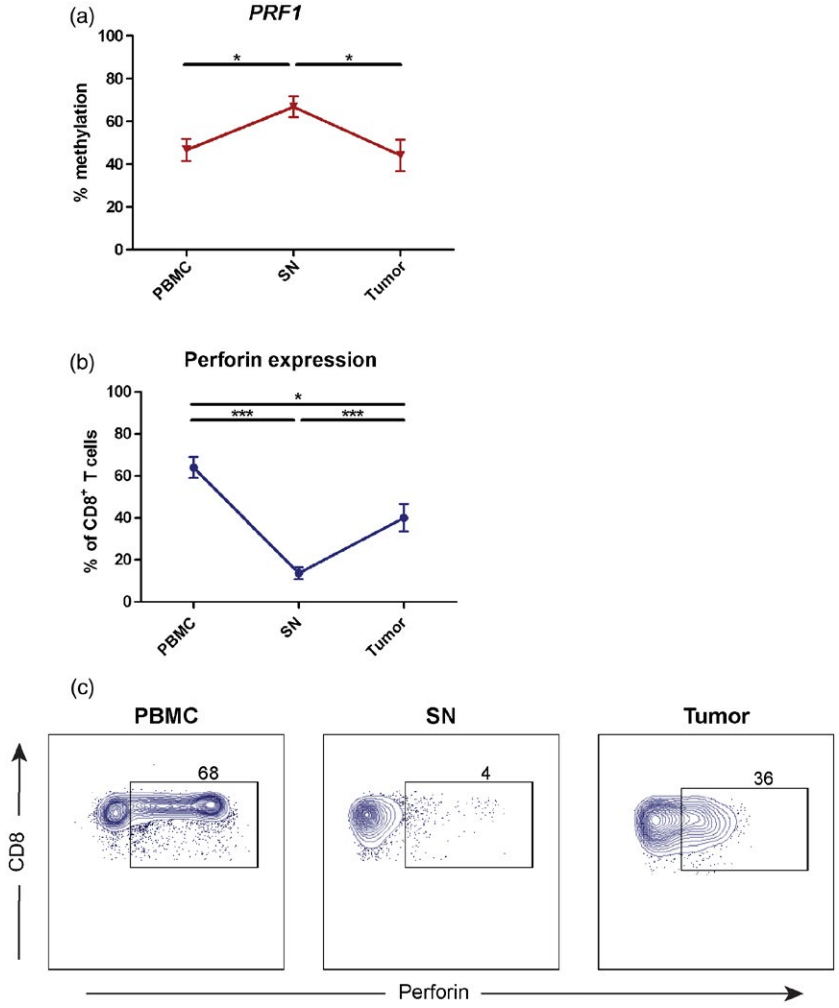

Fig. 2. Distinct epigenetic regulation of perforin in CD8$^+$ T cells from different tissues. (a) DNA methylation profile of *PRF1* reporter cytosine–phosphate–guanine (CpG) site (–1053) was measured by pyrosequencing of polymerase chain reaction (PCR)-amplified bisulfite-converted DNA isolated from CD8$^+$ T cells from peripheral blood mononuclear cells (PBMC), sentinel nodes (SN) and tumour (n = 15). The data are the mean with error bars indicating standard error of the mean (s.e.m.); one-way analysis of variance (ANOVA) was used as the statistical test. (b) The frequency of perforin$^+$ CD8$^+$ T cells from PBMC, SN and tumour (n = 25) was measured by flow cytometry. The data are the mean with error bars indicating s.e.m.; Kruskal–Wallis was used as the statistical test. (c) The expression of perforin in CD8$^+$ T cells from different tissues (n = 25) were measured by flow cytometry. The gate was based on isotype control and the frequency of perforin$^+$ cells was counted out of CD8$^+$ T cells. Dot-plots display representative data from one patient. *P < 0·05, **P < 0·01, ***P < 0·001, ****P < 0·0001.

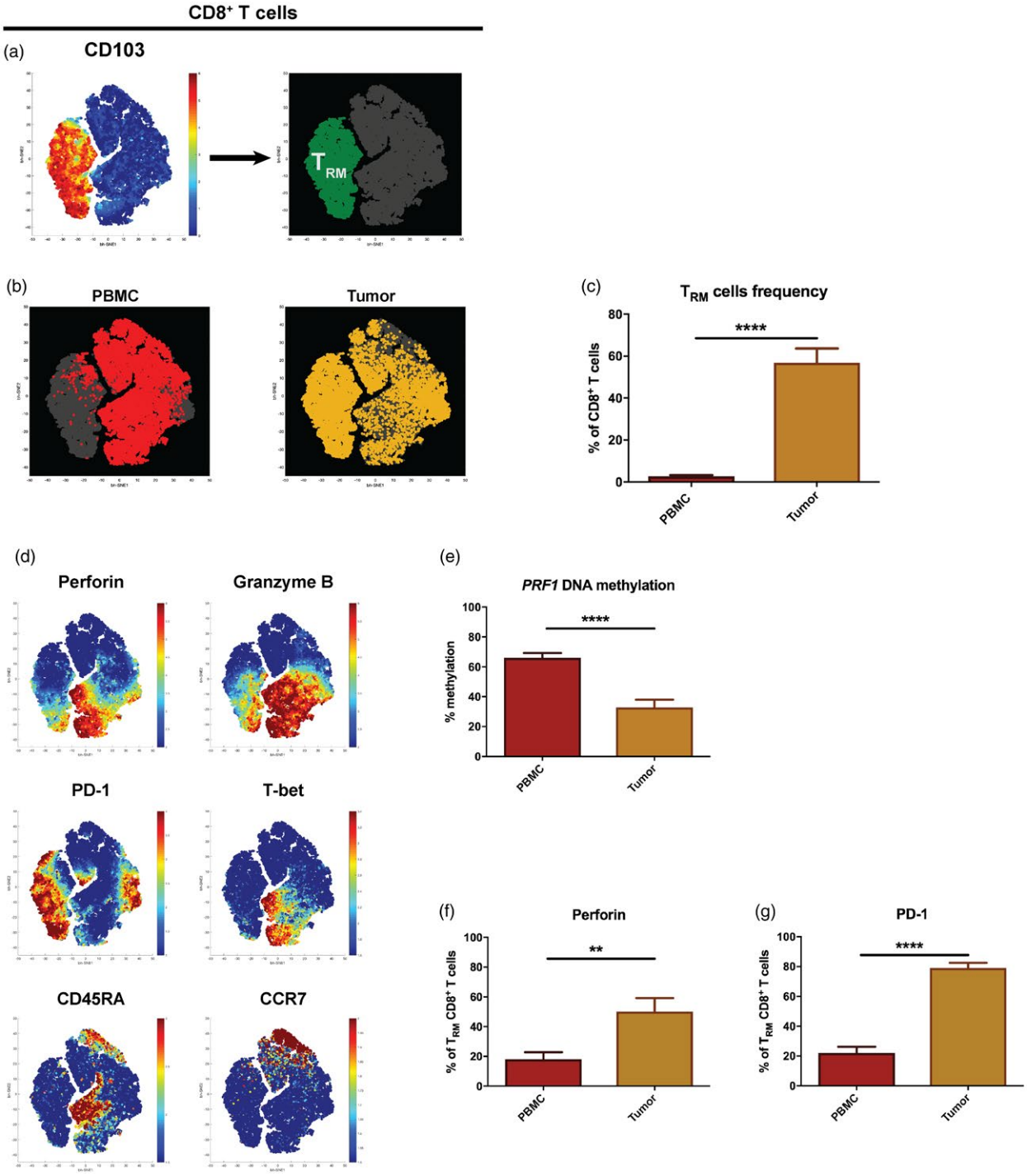

Fig. 3. Cytotoxic tissue-resident memory T cells in tumour despite of exhaustion. (a) ViSNE analysis was performed from flow cytometry data of $CD8^+$ T cells from peripheral blood mononuclear cells (PBMC) and tumour (n = 8). Tissue-resident memory T (T_{RM}) cells are indicated in green based on CD103 expression. (b) ViSNE analysis of $CD8^+$ T cells derived from PBMC and tumour (n = 8) were plotted (red = PBMC and yellow = tumour). (c) T_{RM} cell frequency in PBMC and tumour (n = 13) were measured by flow cytometry and counted out of total $CD8^+$ T cells. The bar graph shows the mean with error bars indicating standard error of the mean (s.e.m.). Independent t-test was used as statistical test. (d) The parameter expressions, in which the algorithm of ViSNE in (a,b) was calculated, are displayed with colour indicator representing fluorescence intensity (n = 8). (e) DNA methylation profile of *PRF1* reporter cytosine–phosphate–guanine site (CpG) site (–1053) was measured by pyrosequencing of polymerase chain reaction (PCR)-amplified bisulfite-converted DNA isolated from T_{RM} cells of PBMC and tumour (n = 10). The bar graph shows the mean with error bars indicating s.e.m.; independent t-test was used as statistical test. (f,g) Fraction of perforin$^+$ T_{RM} cells or programmed cell death 1 (PD-1)$^+$ T_{RM} cells in PBMC and tumour (n = 8) were measured by flow cytometry. The bar graph shows the mean with error bars indicating s.e.m.; independent t-test was used as statistical test. $^*P < 0{\cdot}05$, $^{**}P < 0{\cdot}01$, $^{***}P < 0{\cdot}001$, $^{****}P < 0{\cdot}0001$.

compared to PBMC and tumour (both $P < 0{\cdot}05$) (Fig. 2a).

To validate the DNA methylation status to the expression of perforin, we performed flow cytometry on $CD8^+$ T cells from UBC patients. Correspondingly, the number of perforin-expressing $CD8^+$ T cells was nine times higher in tumour ($P < 0{\cdot}001$) and 17 times higher in PBMC ($P < 0{\cdot}001$) in comparison to SN (Fig. 2b and c). In addition, there was a significant difference between the frequency of perforin$^+$ $CD8^+$ T cells from tumour and PBMC ($P = 0{\cdot}01$) (Fig. 2b). The findings indicate epigenetic regulation of the $CD8^+$ T cell phenotype in different tissues with regard to the cytotoxic constituent perforin.

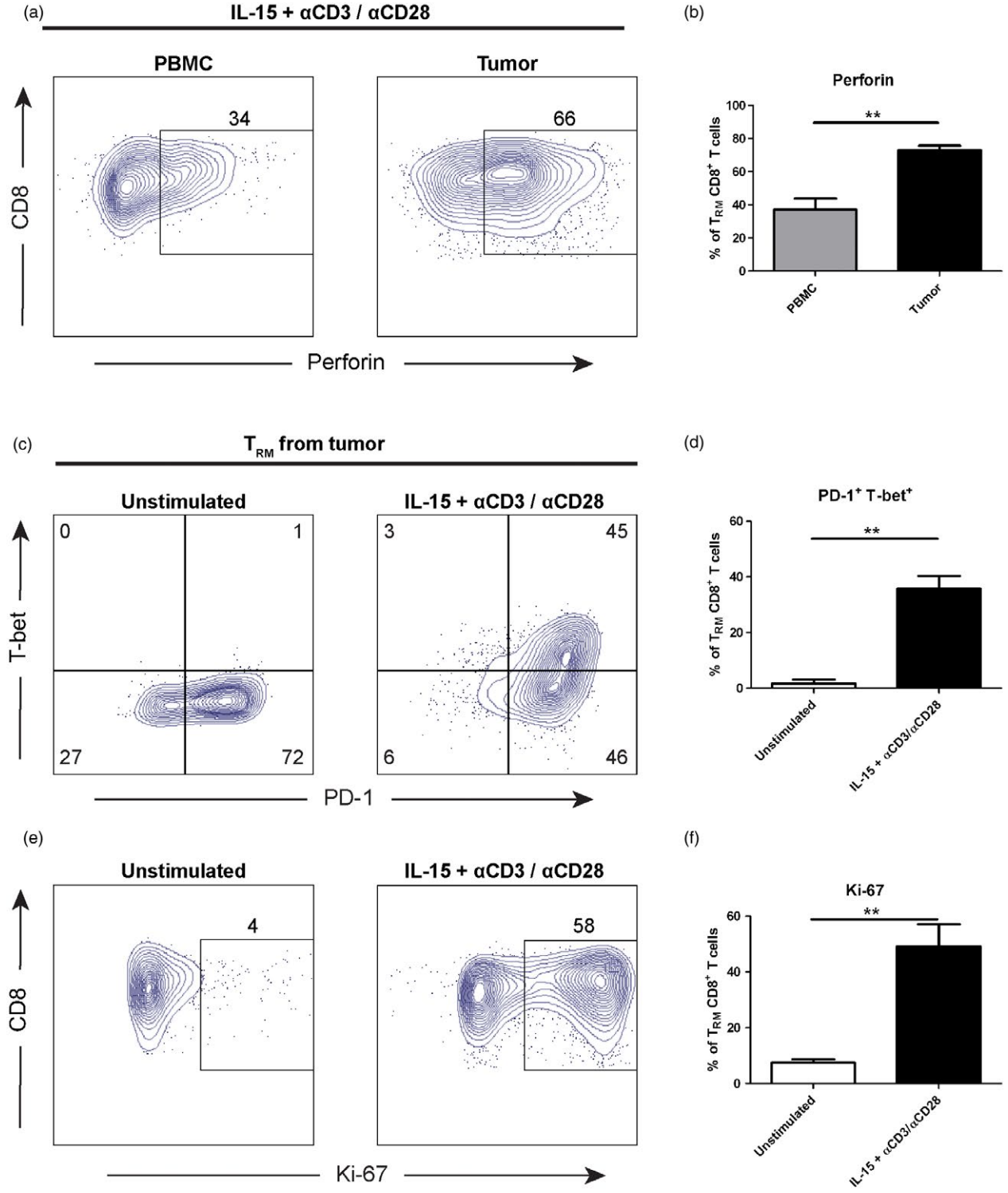

Fig. 4. Tissue-resident memory T cells in tumour are not terminally exhausted. (a) Tissue-resident memory T (T_{RM}) cells from peripheral blood mononuclear cells (PBMC) and tumour ($n = 3$) were activated using 20 ng/ml recombinant human interleukin (IL)-15, 5 μg/ml plate-coated anti-CD3 and 1 μg/ml anti-CD28 stimulating antibodies for 48 h. The expression of perforin post-stimulation was measured by flow cytometry. The gate was based on isotype control and the frequency of perforin$^+$ cells was counted out of T_{RM} cells. Dot-plots display representative data from one patient. (b) The frequency of perforin$^+$ T_{RM} cells in PBMC and tumour ($n = 3$) from (a) is shown. The bar graph demonstrate the mean with error bars indicating standard error of the mean (s.e.m.); independent *t*-test was used as statistical test. (c) The expression of T-bet and programmed cell death 1 (PD-1) in T_{RM} cells from tumour ($n = 3$) were measured by flow cytometry post-culture, comparing unstimulated and stimulated groups. The gate was based on isotype control. Dot-plots display representative data from one patient. (d) The frequency of PD-1$^+$ T-bet$^+$ T_{RM} cells in unstimulated and stimulated groups ($n = 3$) from (c) is shown. The bar graph shows the mean with error bars indicating s.e.m.; independent *t*-test was used as statistical test. (e) The same as in (c), but the dot-plots show the expression of Ki-67 in T_{RM} cells ($n = 3$). (f) Same as in (d), but the graph shows the frequency of Ki-67$^+$ T_{RM} cells from (e) ($n = 3$). $^*P < 0{\cdot}05$, $^{**}P < 0{\cdot}01$, $^{***}P < 0{\cdot}001$, $^{****}P < 0{\cdot}0001$.

Tissue-resident memory T cells in tumour are cytotoxic but exhausted

To explore further potential phenotypical differences between CD8$^+$ T cells from tumour and PBMC, not revealed by DNA methylation of the *PRF1* locus (Fig. 2a), we characterized memory CD8$^+$ T cell subsets using flow cytometry and ViSNE analysis. Tissue-resident memory T (T_{RM}) cells, based on CD103 expression (Fig. 3a), were discovered to be increased significantly in the tumour (mean = 56·8%) compared to PBMC (mean = 2·7%) ($P < 0{\cdot}0001$) (Fig. 3b and c). Interestingly, a small number of T_{RM} cells could be observed both in the blood (PBMC) of UBC patients and healthy individuals (Supporting information, Fig. S1).

Furthermore, DNA methylation of the *PRF1* reporter CpG site (–1053) in tumour-derived T_{RM} cells was decreased twofold compared to PBMC ($P < 0{\cdot}0001$) (Fig. 3e). Consequently, perforin-expressing T_{RM} cells were increased in tumours ($P = 0{\cdot}008$) (Fig. 3d and f). In addition, we found that the fraction of T_{RM} cells expressing granzyme B was increased in the tumours compared to PBMC ($P < 0{\cdot}001$) (Fig. 3d, Supporting information, Fig. S2a).

The tumour contained a significantly higher number of T_{RM} cells that expressed the exhaustion marker PD-1 compared to PBMC (mean tumour = 79% *versus* mean PBMC = 21·9%) ($P < 0{\cdot}0001$) (Fig. 3d and g). Additionally, T-bet expression was low in tumours (Fig. 3d, Supporting information, Fig. S2b), suggesting exhaustion of tumour-derived T_{RM} cells.

Tissue-resident memory T cells can be activated despite signs of exhaustion

In order to investigate the functional capacity of T_{RM} cells despite the signs of exhaustion (high PD-1 and low T-bet expression), we activated T_{RM} cells from tumour and PBMC with IL-15 in the presence of anti-CD3 and anti-CD28 stimulating antibodies. Following 48 h of stimulation, the number of perforin-expressing T_{RM} cells from the tumour increased twofold compared to PBMC ($P = 0{\cdot}008$) (Fig. 4a and b), with no difference in the proportion of granzyme B$^+$, PD-1$^+$ and T-bet$^+$ cells (Supporting information, Fig. S3). No prominent change in the DNA methylation of *PRF1* signature locus was observed (Supporting information, Fig. S4).

Moreover, the frequency of T_{RM} cells expressing PD-1$^+$ T-bet$^+$ increased 21 times following stimulation ($P = 0{\cdot}002$) (Fig. 4c and d). Additionally, Ki-67 expression was elevated significantly in stimulated T_{RM} cells, demonstrated by a 6·6 times increase after IL-15 and T cell receptor (TCR)-stimulation ($P = 0{\cdot}007$) (Fig. 4e and f). Taken together, PD-1-expressing T_{RM} cells from the tumour possessed great cytotoxic and proliferative potential following activation of the cells, demonstrating that they are not terminally exhausted.

Tissue-resident memory T cells are the most dominant subset in the tumour

As we have demonstrated the cytotoxic and functional capacity of T_{RM} cells when they resided in the tumour, the next step was to compare the phenotype of T_{RM} cells to other memory cell subsets present. ViSNE analysis was performed on total CD8$^+$ T cells isolated from the tumour. As mentioned earlier, T_{RM} cells co-expressed CD49a and CD69 alongside CD103 and constituted the dominant memory cell subset in the tumour ($P < 0{\cdot}001$) (Fig. 5a and b). However, other memory cell subsets were also present, such as central memory T (T_{CM}) cells (CD103$^-$ CD45RA$^-$CCR7$^+$, mean = 4·25%), effector memory T (T_{EM}) cells (CD103$^-$CD45RA$^-$CCR7$^-$, mean = 27·3%) and effector memory T cells with CD45RA up-regulation (T_{EMRA}) (CD103$^-$CD45RA$^+$CCR7$^-$, mean = 8·7%) (Fig 5a and b).

When investigating the DNA methylation profile of the *PRF1* reporter CpG site (–1053) in each cell subset, T_{RM} cells and T_{EM} cells demonstrated intermediate methylation (mean = 32·9 and 42·6%, respectively) with significant lower to T_{CM} cells, but higher when compared to T_{EMRA} cells (Fig. 5c). This corresponded inversely with the number of perforin$^+$ cells among T_{RM} and T_{EM} cells, which was significantly higher compared to T_{CM} cells ($P < 0{\cdot}01$) and lower than terminally differentiated T_{EMRA} cells ($P < 0{\cdot}05$) (Fig. 5d). This expression pattern was also observed for granzyme B (Supporting information, Fig. S5).

The fraction of PD-1-expressing cells was the highest among T_{RM} cells when compared to other cell subsets ($P < 0{\cdot}001$) (Fig. 5e, left panel), which resulted consequently in a significantly lower expression of T-bet ($P = 0{\cdot}014$ T_{RM} *versus* T_{EMRA}) (Fig. 5e, right panel). We conclude that the T_{RM} cells are dominant in the tumours

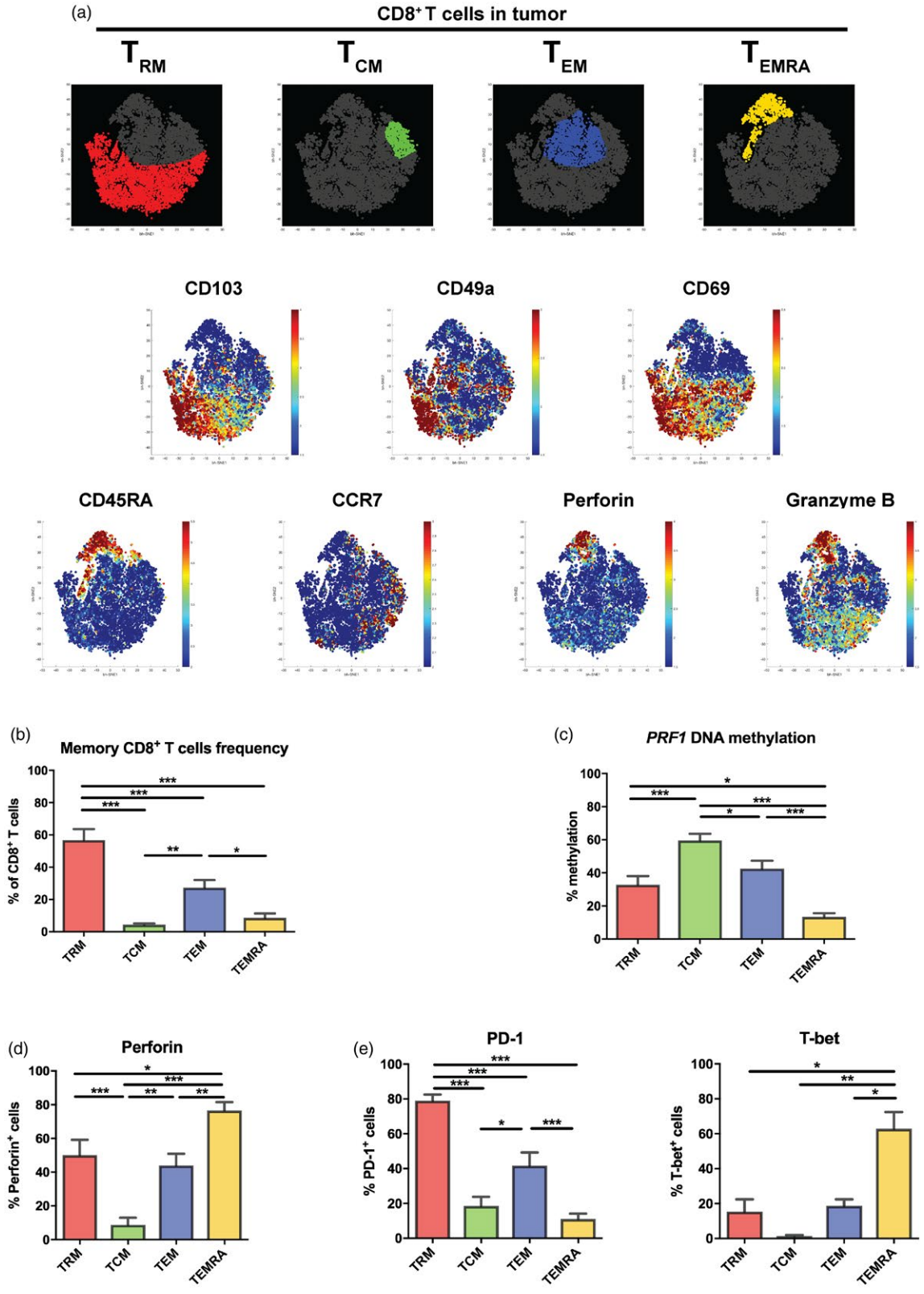

Fig. 5. Tumour tissue is highly infiltrated by tissue-resident memory T cells. (a) ViSNE analysis was performed on tumour $CD8^+$ T cells data measured by flow cytometry ($n = 4$). Distinct $CD8^+$ T cell memory subsets were plotted [red = tissue-resident memory T (T_{RM}), green = T_{CM}, blue = T_{EM} and yellow = T_{EMRA}]. The parameter expressions, in which the algorithm of ViSNE was calculated, are displayed with colour indicator representing fluorescence intensity. (b) The frequency of memory $CD8^+$ T cell subsets were measured by flow cytometry and counted out of total $CD8^+$ T cells ($n = 13$). The bar graph shows the mean with error bars indicating standard error of the mean (s.e.m.); one-way analysis of variance (ANOVA) was used as statistical test. (c) DNA methylation profile of *PRF1* reporter cytosine–phosphate–guanine (CpG site) (−1053) was measured by pyrosequencing of polymerase chain reaction (PCR)-amplified bisulfite-converted DNA isolated from different tumour memory $CD8^+$ T cell subsets ($n = 10$). The bar graph shows the mean with error bars indicating s.e.m.; one-way ANOVA was used as statistical test. (d,e) Fraction of perforin$^+$, programmed cell death 1 (PD-1)$^+$ or T-bet$^+$ in different memory $CD8^+$ T cell subsets were measured by flow cytometry ($n = 8$). The bar graph shows the mean with error bars indicating s.e.m.; one-way ANOVA was used as statistical test. $^*P < 0{\cdot}05$, $^{**}P < 0{\cdot}01$, $^{***}P < 0{\cdot}001$, $^{****}P < 0{\cdot}0001$.

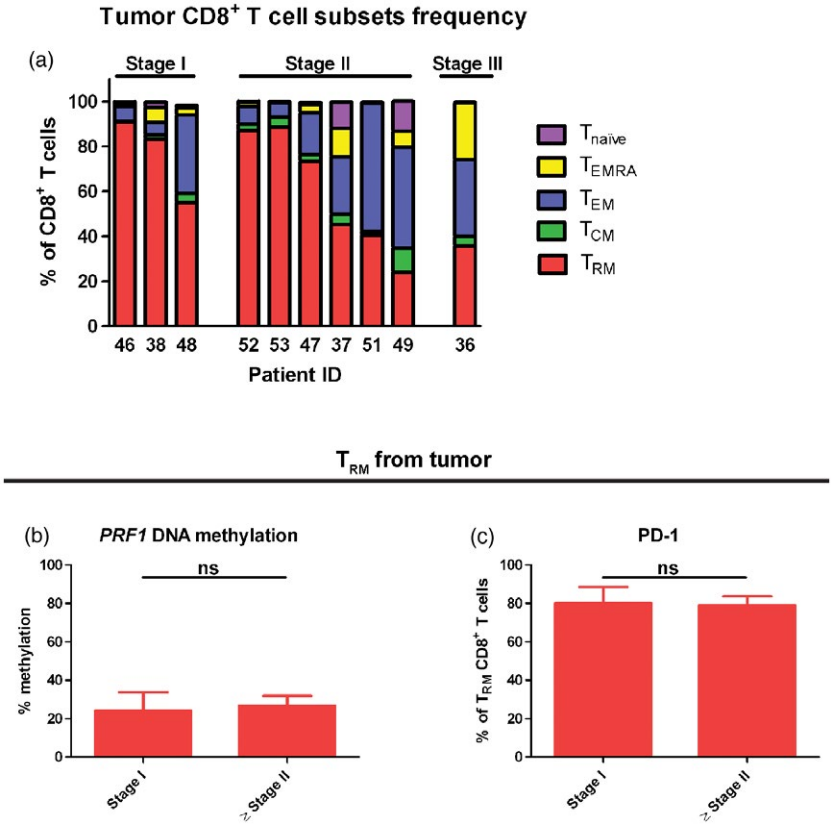

Fig. 6. The increased number of tissue-resident memory T (T_{RM}) cells in tumours correlates with lower tumour stage. (a) The proportion of distinct memory $CD8^+$ T cell subsets in the tumour was measured by flow cytometry and displayed from each urinary bladder cancer (UBC) patient ($n = 10$). Patients were grouped based on the tumour–node–metastasis (TNM) tumour stage judged clinically. Stage I = T1 N0 M0, stage II = T2 N0 M0 and stage III = T3 N0 M0. (b) DNA methylation profile of *PRF1* reporter cytosine–phosphate–guanine (CpG) site (−1053) was measured by pyrosequencing of polymerase chain reaction (PCR)-amplified bisulfite-converted DNA isolated from tumour T_{RM} cells and compared between patients with stage I and ≥ stage II ($n = 10$). The bar graph shows the mean with error bars indicating standard error of the mean (s.e.m.); Mann–Whitney was used as statistical test. (c) The frequency of programmed cell death 1 (PD-1)$^+$ T_{RM} cells from tumour was measured by flow cytometry and compared between patients with stage I and ≥ stage II ($n = 10$). The bar graph shows the mean with error bars indicating s.e.m.; Mann–Whitney was used as statistical test.

demonstrating higher cytotoxic quality compared to the other cell subsets.

High infiltration of tumour tissue-resident memory T cells corresponds with lower tumour stage

Because T_{RM} cells were demonstrated to have positive cytotoxic properties, we correlated the proportion of different memory $CD8^+$ T cell subsets infiltrating the tumour to clinical tumour–node–metastasis (TNM) stage in UBC patients. We observed that in the patients with stage I (T1 N0 M0), there was a trend towards dominant T_{RM} cell infiltration in the tumour (Fig. 6a). Notably, patient 48 had a lower T_{RM} cell number, similar to high-stage tumour. Hypothetically, it was due to the high-risk

stage I tumour (cT1 + carcinoma *in situ*) in this patient. In contrast, in patients with muscle invasive tumour, i.e. stage II (T2 N0 M0) and stage III (T3 N0 M0), the trend demonstrated a lower fraction of T_{RM} cells in the tumour (Fig. 6a).

Furthermore, when comparing DNA methylation in the *PRF1* locus, there was no significant difference between patients with non-muscle invasive (stage I) and muscle-invasive (≥ stage II) tumours (P = 0·571) (Fig. 6b). In addition, the PD-1-expressing T_{RM} cell number was not seen to be different between the two stage groups (P = 1·0) (Fig. 6c). This suggests that the tumour T_{RM} cells have similar phenotypes among tumour stages.

Discussion

Here, for the first time to our knowledge, we demonstrated that phenotypically exhausted T_{RM} cells are epigenetically available for the transcription of perforin and harbour effector functions, which may correlate with a less advanced tumour stage. Our findings suggest that T_{RM} cells residing in the tumour tissue of urothelial UBC have low DNA methylation in the reporter CpG site located in the enhancer of the *PRF1* locus (Fig. 3e). This discovery has a solid correlation with the perforin protein expression inside the cells (Fig. 3f) and renders the possibility to activate tumour T_{RM} cells (Fig. 4). Moreover, a high number of T_{RM} cells infiltrating the tumour corresponds to a lower tumour stage in UBC patients (Fig. 6a). Epigenetic profiling of T_{RM} cells may help us in revealing mechanisms that can be targeted to reverse exhaustion and enhance cytotoxic potency in future cancer immunotherapy regimens.

The rationale for investigating the enhancer region of the *PRF1* gene relies on the fact that the regulation by enhancers are proven to be highly dynamic upon $CD8^+$ T cell activation and differentiation [24]. Furthermore, the transcription of *PRF1* is regulated mainly by the enhancer located at position –1kb from the TSS, which has binding sites for transcription factors related to T cell activation, such as signal transducer and activator of transcription (STAT)-5, nuclear factor kappa B (NF-κB) and activator protein 1 (AP-1) [25]. Hence, it is compelling to examine the DNA methylation status of the CpG signature site in the enhancer region, where we found a good correlation with perforin expression (Fig. 2). However, we observed that *PRF1* methylation was equivalent in PBMC and tumour $CD8^+$ T cells, but the perforin protein expression is lower in the tumour (Fig. 2). This discrepancy may be due to additional mechanisms that regulate perforin expression, such as microRNAs [26] or histone modifications.

It is widely acknowledged that DNA methylation has a critical role in gene expression and specific cell lineage maintenance. Therefore, DNA methylation establishes a stable epigenetic mark which can be inherited through successive cell divisions [27]. In the context of $CD8^+$ T cell differentiation, a shift in DNA methylation is not a straightforward phenomenon once $CD8^+$ T cells have retained their specific memory subset. Accordingly, effector-associated loci, such as *PRF1*, have a stably unchanged DNA methylation in peripheral blood-derived naive, T_{CM} and T_{EM} $CD8^+$ T cells, even after three rounds of cell division by *ex-vivo* stimulation using homeostatic cytokines IL-7 and IL-15 [28].

These insights prompted us to study DNA methylation of the *PRF1* locus in tissue-resident memory T (T_{RM}) cells, which have unique transcriptional signatures compared to T_{CM} and T_{EM} cells [3]. T_{RM} cells are defined as memory $CD8^+$ T cells that reside in the non-lymphoid tissues and have a distinct functional profile [29]. Here, we demonstrated that the *PRF1* locus of T_{RM} cells was hypomethylated compared to T_{CM} and T_{EM} cells from the tumour (Fig. 5c), which corresponded to an increased fraction of perforin-expressing T_{RM} cells (Fig. 5d). Although we could see that terminally differentiated T_{EMRA} cells displayed the lowest DNA methylation in the *PRF1* locus, leading to consequently higher perforin expression compared to T_{RM} cells, we know that T_{EMRA} cells are short-lived in contrast to T_{RM} cells [30]. Moreover, long-lived T_{RM} cells are demonstrated to elicit more potent local immune protection in the tissue against infection [31].

In cancer, T_{RM} cells are reported to delay tumour growth and prolong survival [32]. Additionally, T_{RM} cells are necessary for the efficacy of cancer vaccine [11,33]. The protective effect of T_{RM} cells in cancer is linked to their high degree of cytotoxicity, which is correlated with the magnitude of their perforin and granzyme expression [14]. In spite of expressing cytotoxic mediators, T_{RM} cells in the tumour express the exhaustion markers PD-1, T cell immunoglobulin and mucin domain 3 (TIM-3) and lymphocyte-activation gene 3 (LAG-3) [34]. In accordance with these previous findings, in this study we have demonstrated a high number of PD-1^+ T_{RM} cells from the tumour (Fig. 3g) and a low fraction of T-bet^+ cells in this subset (Supporting information, Fig. S2b). However, when we activated T_{RM} cells from tumours using the homeostatic cytokine IL-15 and T cell receptor (TCR) stimulation *in vitro*, we observed that the dominant PD-1^+ T_{RM} cells began to gain T-bet expression (Fig. 4c and d). Consequently, this resulted in elevated perforin and granzyme B expression in T_{RM} cells from tumour and increased proliferation, i.e. elevated Ki-67 (Fig. 4e and f). Taken

together, this indicates that the tumour-derived T_{RM} cells are not terminally exhausted. Consistent with our data, skin T_{RM} cells have been described to have high expression of PD-1 and other co-inhibitory molecules after viral infection, thus suggesting exhaustion. Surprisingly, following antigenic challenge, *in-situ* proliferation of T_{RM} cells, marked by up-regulation of Ki-67, occurs [35]. Therefore, we may speculate that the T_{RM} cell is a memory $CD8^+$ T cell subset with an outstanding potential for cytotoxicity and is not terminally exhausted.

The mechanism behind the co-expression of exhaustion markers and cytotoxic mediators seen in T_{RM} cells may be explained as part of T cell activation [36]. We know that PD-1 expression in $CD8^+$ T cells results from chronic antigenic exposure in the tumour tissue [37]. However, recent evidence describes that in the case of chronic infection, permanent PD-1 expression in T_{RM} cells is imprinted epigenetically and is antigen-independent [38,39]. Additionally, PD-1 signalling has been demonstrated to be important for antigen-independent maintenance of memory $CD8^+$ T cells [40]. Therefore, we may speculate that PD-1 expression is a mere T_{RM} cell marker that does not affect cell functionality, and may be seen as an engagement marker with tumour cells. Accordingly, it was seen in our data that PD-1 expression was similar at different stages of the tumour (Fig. 6c).

Notably, our finding indicated that T_{RM} cells present in the peripheral circulation had the capacity to increase their expression of granzyme B, PD-1 and T-bet, following IL-15 and TCR stimulation. The results were comparable to tumour T_{RM} cells (Supporting information, Fig. S3). It is important to note that in this context PD-1 acts as an indicator of T cell activation instead of exhaustion [41]. Therefore, T_{RM} cells from the circulation may have a promising feature of activation following TCR engagement and possibly CD103/E-cadherin ligation once they lodge in the tumour tissue [6,42,43]. However, their specificity towards distinct tumour antigens needs to be investigated further.

The limitation of this study was that we correlated T_{RM} cell numbers with the tumour stage in only 10 patients. However, from this observation we could recapitulate the trend in which high T_{RM} cell infiltration in the tumours corresponded to less advanced tumour stage, suggesting the potential anti-tumour capacity of T_{RM} cells. Therefore, further correlation between patients' clinical prognosis with T_{RM} cell numbers is required in a larger cohort.

In conclusion, epigenetic profiling adds to our understanding about T_{RM} cell phenotypes and functionality. These findings help us to recognize the cytotoxic potential of T_{RM} cells and therefore provide us with new strategies for cancer immunotherapy.

Acknowledgements

This paper was supported by the Swedish Cancer Society (Cancerfonden), the Regional Research Council in Uppsala-Örebro region, Sweden (RFR in Uppsala-Örebro), the Swedish Research Council funding for clinical research in medicine (ALF) in Västerbotten, VLL, Sweden, the Cancer Research Foundation in Norrland, Umeå, Sweden and the Stiftelsen Emil Anderssons fond för medicinsk forskning, Sundsvall, Sweden. The authors acknowledge research nurses Britt-Inger Dahlin and Kerstin Almroth (Department of Surgical and Perioperative Sciences, Urology and Andrology, Umeå University) for their great assistance in this work.

Disclosure

None.

Author contributions

C. A. H., A. S. and O. W. designed the study, developed the methodology, wrote and reviewed the manuscript. C. A. H, E. A. B., A. B. and S. B. performed the experiments. M. J., F. A., T. J., Y. H., F. A., K. P., B. H., K. R. and A. S. provided clinical samples and patients' clinical information. A. S. assembled the clinical information database of all patients. C. A. H. and S. B. performed data analysis. H. G. supervised the study.

References

1 Mueller SN, Mackay LK. Tissue-resident memory T cells: local specialists in immune defence. Nat Rev Immunol 2016;**16**:79–89.

2 Watanabe R, Gehad A, Yang C *et al.* Human skin is protected by four functionally and phenotypically discrete populations of resident and recirculating memory T cells. Sci Transl Med 2015;7. doi:https://doi.org/10.1126/scitranslmed.3010302.

3 Mackay LK, Rahimpour A, Ma JZ *et al.* The developmental pathway for CD103(+)CD8(+) tissue-resident memory T cells of skin. Nat Immunol 2013;**14**:1294–301.

4 Cheuk S, Schlums H, Serezal IG *et al.* CD49a expression defines tissue-resident CD8(+) T cells poised for cytotoxic function in human skin. Immunity 2017;**46**:287–300.

5 Mokrani M, Klibi J, Bluteau D, Bismuth G, Mami-Chouaib F. Smad and NFAT pathways cooperate to induce CD103 expression in human CD8 T lymphocytes. J Immunol 2014;**192**:2471–79.

6 Le Floc'h A, Jalil A, Vergnon I *et al.* alpha(E)beta(7) integrin interaction with E-cadherin promotes antitumor CTL activity by triggering lytic granule polarization and exocytosis. J Exp Med 2007;**204**:559–70.

7 Wang B, Wu SX, Zeng H *et al.* CD103(+) tumor infiltrating lymphocytes predict a favorable prognosis in urothelial cell carcinoma of the bladder. J Urol 2015;**194**:556–62.

8 Djenidi F, Adam J, Goubar A *et al*. CD8(+) CD103(+) tumor-infiltrating lymphocytes are tumor-specific tissue-resident memory T cells and a prognostic factor for survival in lung cancer patients. J Immunol 2015;**194**:3475–86.

9 Komdeur FL, Prins TM, van de Wall S *et al*. CD103+tumor-infiltrating lymphocytes are tumor-reactive intraepithelial CD8+T cells associated with prognostic benefit and therapy response in cervical cancer. Oncoimmunology 2017;**6**: e1338230.

10 Webb JR, Milne K, Watson P, deLeeuw RJ, Nelson BH. Tumor-infiltrating lymphocytes expressing the tissue resident memory marker CD103 are associated with increased survival in high-grade serous ovarian cancer. Clin Cancer Res 2014;**20**:434–44.

11 Nizard M, Roussel H, Diniz MO *et al*. Induction of resident memory T cells enhances the efficacy of cancer vaccine. Nat Commun 2017;**8**. doi: https://doi.org/10.1038/ncomms15221.

12 Schenkel JM, Fraser KA, Vezys V, Masopust D. Sensing and alarm function of resident memory CD8(+) T cells. Nat Immunol 2013;**14**:509–13.

13 Cullen SP, Brunet M, Martin SJ. Granzymes in cancer and immunity. Cell Death Diff 2010;**17**:616–23.

14 Ganesan AP, Clarke J, Wood O *et al*. Tissue-resident memory features are linked to the magnitude of cytotoxic T cell responses in human lung cancer. Nat Immunol 2017;**18**:940–50.

15 Allis CD, Jenuwein T. The molecular hallmarks of epigenetic control. Nat Rev Genet 2016;**17**:487–500.

16 Schubeler D. Function and information content of DNA methylation. Nature 2015;**517**:321–26.

17 Arner E, Daub CO, Vitting-Seerup K *et al*. Transcribed enhancers lead waves of coordinated transcription in transitioning mammalian cells. Science 2015;**347**:1010–14.

18 Henning AN, Roychoudhuri R, Restifo NP. Epigenetic control of CD8+ T cell differentiation. NatRev Immunol 2018;**18**: 340–56.

19 Burger M, Catto JW, Dalbagni G, *et al*. Epidemiology and risk factors of urothelial bladder cancer. Eur Urol 2013;**63**:234–41.

20 Redelman-Sidi G, Glickman MS, Bochner BH. The mechanism of action of BCG therapy for bladder cancer-a current perspective. Nat Rev Urol 2014;**11**:153–62.

21 Rosenblatt R, Johansson M, Alamdari F *et al*. Sentinel node detection in muscle-invasive urothelial bladder cancer is feasible after neoadjuvant chemotherapy in all pT stages, a prospective multicenter report. World J Urol 2017;**35**:921–27.

22 Amir ED, Davis KL, Tadmor MD *et al*. viSNE enables visualization of high dimensional single-cell data and reveals phenotypic heterogeneity of leukemia. Nat Biotechnol 2013;**31**:545–52.+.

23 Lu QJ, Wu AL, Ray D *et al*. DNA methylation and chromatin structure regulate T cell perforin gene expression. J Immunol 2003;**170**:5124–32.

24 He B, Xing SJ, Chen CY *et al*. CD8(+) T cells utilize highly dynamic enhancer repertoires and regulatory circuitry in response to infections. Immunity 2016;**45**:1341–54.

25 Pipkin ME, Rao A, Lichtenheld MG. The transcriptional control of the perforin locus. Immunol Rev 2010;**235**:55–72.

26 Trifari S, Pipkin ME, Bandukwala HS *et al*. MicroRNA-directed program of cytotoxic CD8+ T-cell differentiation. Proc Natl Acad Sci USA 2013;**110**:18608–13.

27 Cedar H, Bergman Y. Programming of DNA methylation patterns. Ann Rev Biochem 2012;**81**:97–117.

28 Abdelsamed HA, Moustaki A, Fan YP *et al*. Human memory CD8 T cell effector potential is epigenetically preserved during in vivo homeostasis. J Exp Med 2017;**214**:1593–606.

29 Sathaliyawala T, Kubota M, Yudanin N *et al*. Distribution and compartmentalization of human circulating and tissue-resident memory T cell subsets. Immunity 2013;**38**:187–97.

30 Sallusto F, Geginat J, Lanzavecchia A. Central memory and effector memory T cell subsets: function, generation, and maintenance. Ann Rev Immunol 2004;**22**:745–63.

31 Mackay LK, Stock AT, Ma JZ *et al*. Long-lived epithelial immunity by tissue-resident memory T (T-RM) cells in the absence of persisting local antigen presentation. Proc Natl Acad Sci USA 2012;**109**:7037–42.

32 Milner JJ, Toma C, Yu BF *et al*. Runx3 programs CD8(+) T cell residency in non-lymphoid tissues and tumours. Nature 2017;**552**:253–57.

33 Granier C, Blanc C, Karaki S, Tran T, Roussel H, Tartour E. Tissue-resident memory T cells play a key role in the efficacy of cancer vaccines. Oncoimmunology 2017;**6**. doi: https://doi.org/10.1080/2162402X.2017.

34 Webb JR, Milne K, Nelson BH. PD-1 and CD103 are widely coexpressed on prognostically favorable intraepithelial CD8 T cells in human ovarian cancer. Cancer Immunol Res 2015;**3**:926–35.

35 Park SL, Zaid A, Hor JL *et al*. Local proliferation maintains a stable pool of tissue-resident memory T cells after antiviral recall responses. Nat Immunol 2018;**19**:183–91.

36 Kumar BV, Connors TJ, Farber DL. Human T cell development, localization, and function throughout life. Immunity 2018;**48**:202–213.

37 Wherry EJ, Kurachi M. Molecular and cellular insights into T cell exhaustion. Nat RevImmunol 2015;**15**:486–99.

38 Youngblood B, Oestreich KJ, Ha SJ *et al*. Chronic virus infection enforces demethylation of the locus that encodes PD-1 in antigen-specific CD8(+) T cells. Immunity 2011;**35**:400–12.

39 Shwetank Abdelsamed HA, Frost EL, Schmitz HM, Mockus TE, Youngblood BA, Lukacher AE. Maintenance of PD-1 on brain-resident memory CD8 T cells is antigen independent. Immunol Cell Biol 2017;**95**:953–9.

40 Yuzefpolskiy FM, Penny LA, Kalia V, Sarkar S. Signaling through PD-1 on CD8 T cells is critical for antigen-independent maintenance of immune memory. Immunology 2016. J Immunol 2016;**196**(Suppl 1):129.6.

41 Legat A, Speiser DE. Pircher H, Zehn D, Marraco SAF. Inhibitory receptor expression depends more dominantly on differentiation and activation than 'exhaustion' of human CD8 T cells. Front Immunol 2013;**4**:455.

42 Le Floc'h A, Jalil A, Franciszkiewicz K, Validire P, Vergnon I, Mami-Chouaib F. Minimal engagement of CD103 on cytotoxic T lymphocytes with an E-cadherin-Fc molecule triggers lytic granule polarization via a phospholipase C gamma-dependent pathway. Cancer Res 2011;**71**:328–38.

43 Gauthier L, Corgnac S, Boutet M *et al.* Paxillin binding to the cytoplasmic domain of CD103 promotes cell adhesion and effector functions for CD8(+) resident memory T cells in tumors. Cancer Res 2017;**77**:7072–82.

Supporting Information

Additional supporting information may be found in the online version of this article at the publisher's web site:

Fig S1. A small fraction of T_{RM} cells is present in the blood of UBC patients and healthy individuals. ViSNE analysis was performed on PBMC $CD8^+$ T cells data measured by flow cytometry (n = 7). Tissue-resident memory T (T_{RM}) cells are indicated in green based on CD103 expression. PBMC $CD8^+$ T cells from healthy donors and UBC patients were plotted (red = healthy donors and yellow = UBC patients).

Fig S2. Cytotoxic tissue-resident memory T cells in tumour despite of exhaustion. (a) The frequency of granzyme B^+ T_{RM} cells in PBMC and tumour (n = 8) were measured by flow cytometry and counted out of T_{RM} cells. The bar graph shows means with error bars indicating SEM. Independent t-test was used as statistical test. (b) Same as in (a), but the data show T-bet^+ T_{RM} cell frequency (n = 8). Mann-Whitney was used as statistical test. $^*P < 0{\cdot}05$, $^{**}P < 0{\cdot}01$, $^{***}P < 0{\cdot}001$, $^{****}P < 0{\cdot}0001$.

Fig S3. T_{RM} cells from blood can potentially be activated. (a) The frequency of granzyme B^+ T_{RM} cells from PBMC and tumour (n = 3) in unstimulated and stimulated condition with IL-15, anti-CD3 and anti-CD28 stimulating antibodies were measured by flow cytometry and counted out of T_{RM} cells. The bar graph shows means with error bars indicating SEM. Independent t-test was used as statistical test. (b)(c) Same as in (a), but the data show the frequency of PD-1^+ T_{RM} cells or T-bet^+ T_{RM} cells (n = 3). $^*P < 0{\cdot}05$, $^{**}P < 0{\cdot}01$, $^{***}P < 0{\cdot}001$, $^{****}P < 0{\cdot}0001$.

Fig S4. DNA methylation of *PRF1* locus does not change following activation. DNA methylation profile of *PRF1* reporter CpG site (-1053) was measured by pyrosequencing of PCR-amplified bisulfite-converted DNA isolated from pre-culture, unstimulated and stimulated (IL-15 + αCD3 + αCD28) tumour T_{RM} cells. The data was acquired from one representative patient.

Fig S5. T_{RM} cells are cytotoxic in the tumour. The fraction of tumour-derived memory $CD8^+$ T cell subsets expressing granzyme B were measured by flow cytometry (n = 8). The bar graph shows means with error bars indicating SEM. One-way ANOVA was used as statistical test. $^*P < 0{\cdot}05$, $^{**}P < 0{\cdot}01$, $^{***}P < 0{\cdot}001$, $^{****}P < 0{\cdot}0001$.